THE AMERICAN MINERALOGIST, VOL. 55, JULY-AUGUST, 1970

EDGE-SHARING SILICATE TETRAHEDRA IN THE CRYSTAL STRUCTURE OF LEUCOPHOENICITE

PAUL B. MOORE, *Department of the Geophysical Sciences, University of Chicago, Chicago, Illinois 60637*

ABSTRACT

Leucophoenicite, a 10.842 (19), b 4.826 (6), c 11.324 (9) Å, β 103.93° (9), $P2_1/a$, possesses the crystallochemical formula Mn_7 $[SiO_4]_2[(SiO_4)(OH)_2]$, with two formula units in the crystal cell. The atomic arrangement was deciphered from Patterson synthesis; atomic coordinate and isotropic temperature factor refinement by least-squares techniques led to $R_{hkl}=0.07$, using 1207 non-zero reflections.

The structure is based on hexagonal close-packed oxygen anions stacked parallel to {010}, with an octahedral two-layer repeat. The octahedral populations define a new kind of kinked serrated chain equally apportioned in the two octahedral levels of the b-axis repeat. These chains run parallel to the z-axis, explaining the frequent twinning by reflection on {001}. A family of kinked serrated chains can be defined by a simple algorithm which utilizes a particular octahedral cluster as its component. Leucophoenicite actually belongs to a homologous series distinct from the closely related humite mineral group, although both series have in common the olivine structure type as their simplest member.

The octahedrally populated chains place restrictions on the tetrahedral populations. For leucophoenicite, there is a set of fully occupied tetrahedra with point symmetry 1 and a set of disordered half-occupied tetrahedra; these latter occur as edge-sharing tetrahedral pairs, with the mid-point of the common edge possessing point symmetry $\bar{1}$. This pair has average composition $[(SiO_4)(OH)_2]$ and its presence results in unusual but explicable polyhedral distortions.

INTRODUCTION

Leucophoenicite was a fairly abundant basic manganese silicate which occurred as crystals in late stage open hydrothermal veins and as granular masses in ore and skarn from Franklin, New Jersey, its type locality. It most frequently occurred as interlocking grains of a purplish-pink color, usually in association with green willemite, tephroite, glaucochroite and coarsely crystalline franklinite. The crystals, from a younger and distinctly different paragenesis, are rich raspberry-red in color, rendering the species one of the most beautiful members of the mineral kingdom.

Leucophoenicite was named and first described by Penfield and Warren (1899) during their studies on the paragenesis of a bewildering array of lead-zinc-manganese silicates encountered in the Parker Shaft workings. They interpreted leucophoenicite as a manganese member of the humite group, isotypic to humite. Palache (1910, 1928) presented his results of morphological investigation on fifteen crystals, established the symmetry as monoclinic holosymmetric, and later summarized the leucophoenicite paragenesis in considerable detail (Palache, 1935). In spite of the close

chemical similarity to humite, he concluded that leucophoenicite was not allied to the humite group. Based on Palache's data, a morphological analysis was presented by Moore (1967). He confirmed the monoclinic character of the mineral, but showed that a pseudo-orthorhombic cell could be chosen which was related to humite. Recently, Cook (1969) routinely investigated many specimens labelled "leucophoenicite" and "tephroite" from Franklin and Sterling Hill by X-ray powder diffraction, and further showed that the studies of Palache and Moore were based on more than one species, which included leucophoenicite proper and sonolite.

To add to the complex history of this mineralogical curiosity, Moore (1967) stated that there exists more than one kind of leucophoenicite. Massive pink leucophoenicite yields "orthorhombic" single crystal data which are closely related to the monoclinic cell criteria found for single crystal hydrothermal vein material. Finally, a new species, isotypic to humite and dimorphous to leucophoenicite has been studied recently in my laboratory.

Two wet chemical analyses have been reported for leucophoenicite and are recorded in Table 1 along with a computation of the cell contents. In addition, ARL electron probe analyses performed on regions of the crystal used in this study essentially confirm the earlier analyses. Standards used in the probe study included tephroite (Mn,Si), pyrope (Mg,Al), smithsonite (Zn) and anorthite (Ca). The results, corrected for absorption and atomic number effects, are reported in Table 1. The empirical formula unit is close to $H_2X^{2+}{}_7Si_3O_{14}$, where X is chiefly Mn with variable amounts of Zn and Ca. A detailed three-dimensional crystal structure analysis, discussed in this paper, not only uniquely defines the species but also throws additional light on the crystal chemistry of the hexagonal close-packed silicate minerals. In addition, a novel kind of silicate disorder was revealed, consisting of edge-sharing half-occupied tetrahedral pairs.

Experimental

The crystal (Chicago Natural History Museum Number M-17356) was a nearly equant fragment of 0.01 mm³ volume. Initially, 1108 independent intensities were gathered from the *h*0*l* to *h*3*l* levels up to $2\theta = 60°$ on a manual scintillation counter Weissenberg geometry diffractometer using Zr-filtered Mo radiation. During the final stages of the study, it readily became apparent that a complete data set was necessary, and a new set of data was obtained from the same crystal on a PAILRED automated diffractometer to $2\theta = 70°$, using monochromatic MoK_α radiation. In this manner, 2601 independent intensities were obtained from the *h*0*l* to *h*6*l* levels, of which 1207 were above background error ("non-zero"). Only the non-zero data were used throughout the study and inspection reveals that they represent essentially random selections throughout reciprocal space. These data were processed in the conventional manner to obtain $|F_{obs}|$; no differential absorption correc-

TABLE 1. CHEMICAL ANALYSES FOR LEUCOPHOENICITE[a]

	Weight percent			M.W. in cell			Atoms in cell			Grouped			Ideal
	1	2	3	1	2	3	1	2	3	1	2	3	
SiO_2	27.32±0.93	26.36	25.28	356.53	354.75	340.22	5.93	5.90	5.66				
Al_2O_3	<0.1	—	1.45		—	19.51		— (Al)	0.38	5.93	5.90	6.04	6.00
MnO	62.98±1.40	60.63	60.34	821.89	815.96	812.05	11.59	11.50	11.45				
ZnO	3.30±0.60	3.87	5.35	43.06	52.08	72.00	0.53	0.64	0.88				
MgO	1.76±0.08	0.21	0.30	22.97	2.83	4.04	0.57	0.07	0.10				
CaO	5.11±0.33	5.67	4.26	66.68	76.31	57.33	1.19	1.36	1.02	13.88	13.80	13.88	14.00
Na_2O	<0.1	0.39	0.90	—	5.25	12.11	—	0.17 (Na)	0.39				
K_2O	<0.1	0.24	0.18	—	3.23	2.42	—	0.06 (K)	0.04				
H_2O	[2.64]	2.64	2.10	34.45	35.53	28.26	3.83	3.94 (OH)	3.14	3.83	3.94	3.14	4.00
	[103.11]	100.01	100.16	1345.58	1345.94	1347.94							

1. G R. Zechman, analyst. Electron probe study on crystal investigated in this paper. Assumed water content added in brackets.
2. C. H. Warren, analyst (Penfield and Warren, 1899).
3. Jenkins and Bauer, analyst (Palache, 1935).

[a] Computations based on $V=580.6$ Å^3, $\rho=3.848$ g/cc.

TABLE 2. LEUCOPHOENICITE STRUCTURE CELL

a	10.842(19)
b	4.826(6)
c	11.324(9)
β	103.93°(9)
Space group	$P2_1/a$
Formula	$Mn_7[SiO_4]_2[(SiO_4)(OH)_2]$
Z	2

tion was applied, since the crystal was of favorable shape and dimension, and a rough calculation showed that this correction would be trivial.

Refined crystal cell data, using Mn-filtered Fe radiation, were obtained from the same specimen, suitably ground with a silicon ($a=5.4301$ Å) standard, and prepared as a sphere mount in 114.6 mm diameter Buerger-type powder cameras. The lines were unambiguously indexed on the basis of the relative single crystal intensities, and a least squares refinement of the cell parameters led to the results in Table 2. Table 3 lists the powder data obtained in this study. The space group, $P2_1/a$, is uniquely determined and was ascertained from single crystal film data and reciprocal space scans on PAILRED.

SOLUTION OF THE CRYSTAL STRUCTURE

There are two $H_2Mn_7Si_3O_{14}$ formula units in the crystal cell with space group $P2_1/a$; thus, one manganese position may be arbitrarily placed at the cell origin. Since $[SiO_4]^{4-}$ tetrahedra cannot be centrosymmetric, it was concluded that one set of general positions probably involved half-occupied tetrahedral sites. The Patterson projection, $P(uw)$, revealed a structure based on hexagonal close-packed oxygen atoms with the layers stacked parallel to {010}. The 4.82 Å b-axis suggested a two-octahedral level repeat structure. Vector sets of hexagonal close-packed systems directly define the atomic positions of the anionic frame. Though the positions of the oxygen atoms could be specified without difficulty, it was not easy to decipher the octahedral and tetrahedral site populations. Since the ratio Mn: O=1:2 and the assumed absence of face-sharing octahedra would yield a projection with equal density octahedral populations, the problem reduced to deciphering the occupied tetrahedral topology. The tetrahedral populations were obtained by generating vector sets of various ordered models which conformed to the symmetry of the crystal, until a model yielded vector densities matching the Patterson projection. The tetrahedral site populations thus obtained permitted approximate calculation of the y-coordinates of Mn, Si and O. This is possible, if no face-sharing among occupied polyhedra is assumed, since Mn must be at $y\sim0$ or $\frac{1}{2}$, Si$\sim$0.4 or 0.6, and O$\sim\frac{1}{4}$ or $\frac{3}{4}$. Three-dimensional structure factor calculations then established the correct ordering scheme for the cations.

TABLE 3. LEUCOPHOENICITE POWDER DATA[a]

I/Io	*d*(obs)	*d*(calc)	*hkl*	*I/Io*	*d*(obs)	*d*(calc)	*hkl*
3	5.23	5.26	200[b]	3	1.7494	1.7541	$\bar{1}16$
5	4.36	4.39	110[b]	4	1.7079	1.7130	$\bar{4}23$
3	3.939	3.940	111	4	1.7012	1.7064	512
5	3.612	3.610	$\bar{1}12$			1.6970	$\bar{3}16$
$3\frac{1}{2}$	3.266	3.272	112	1	1.6653	1.6700	601[b]
2	2.967	2.962	$\bar{1}13$	2	1.6392	1.6406	$\bar{5}15$
9	2.877	2.886	$\bar{3}11$	2	1.6167	1.6149	$\bar{2}07$
3	2.741	2.719	$\bar{2}04$[b]			1.6136	206
		2.710	$\bar{4}01$[b]	2	1.5966	1.5940	315
8	2.684	2.683	113	4	1.5714	1.5702	007
4	2.620	2.626	311	4	1.5641	1.5673	$\bar{6}05$
2	2.486	2.490	$\bar{3}13$	3	1.4732	1.4689	$\bar{3}31$
4	2.441	2.441	$\bar{1}14$	2	1.4441	1.4496	$\bar{3}32$
1	2.413	2.413	020	2	1.4199	1.4183	316
5	2.365	2.369	$\bar{2}14$	3	1.3879		
		2.367	213	2	1.3449		
		2.363	$\bar{4}11$	2	1.3191		
2	2.284	2.275	121	2	1.3134		
3	2.204	2.200	$\bar{3}14$[b]	1	1.2593		
		2.177	402[b]	1	1.2258		
1	2.060	2.057	313[b]	3	1.2121		
		2.049	$\bar{1}15$[b]	3	1.1866		
1	1.9730	1.9600	$\bar{5}12$[b]	1	1.1435		
1	1.8908	1.8907	115[b]	2	1.1173		
		1.8868	$\bar{5}13$[b]	3	1.1072		
10	1.8063	1.8048	$\bar{2}24$				
		1.8039	223				
		1.8023	$\bar{4}21$				

[a] Fe/Mn radiation. 114.6 mm camera diameter; Si(a 5.4301 Å) internal.
[b] Reflections excluded from cell refinement.

REFINEMENT

During the early stages of this study, the incomplete manually collected data set was used and the trial model yielded $R_{hkl}=0.40$. Only 582 reflections were non-zero; several cycles of full-matrix atomic coordinate and isotropic temperature factor refinements based on these non-zero data converged to a minimum $R_{hkl}=0.11$. Scattering curves for the half-ionized species Mn^{+}, Si^{2+} and O were obtained from MacGillavry and Rieck (1962). The estimated standard errors in Me–O distances were high (± 0.03 Å) and the isotropic temperature factors for oxygen ranged widely (-0.17 to 1.19 Å^2). A three-dimensional difference

synthesis failed to reveal any anomalous features or explanation for this range.

Consequently, a more complete set of three-dimensional data was collected on PAILRED. R_{hkl} for the 1207 non-zero reflections was initially 0.10 and converged after eight cycles to 0.07, with all parameter shifts within their limits of error. The Me–O distances proved to have satisfactory standard errors ($\pm$0.009 Å) and all temperature factors were positive and with sensible values. Despite the fact that the final atomic coordinates converged within the range of errors for the initial

TABLE 4. LEUCOPHOENICITE. FINAL ATOMIC COORDINATES AND ISOTROPIC TEMPERATURE FACTORS[a]

Atom	x	y	z	B(Å^2)	M[b]
Mn(1)	0	0	0	0.73(3)	2
Mn(2)	0.3149(2)	0.0150(5)	0.1396(2)	.80(3)	4
Mn(3)	.3308(2)	.4942(5)	.4110(2)	.69(3)	4
Mn(4)	.0781(2)	−.0105(5)	.2967(2)	.80(3)	4
Si(1)	.0246(6)	.4144(13)	.4381(5)	.47(8)	2
Si(2)	.1287(3)	.5731(6)	.1439(3)	.32(4)	4
O(1)	.4907(7)	−.2135(17)	.1458(7)	.48(11)	4
O(2)	.3345(8)	.2137(18)	−.0265(7)	.73(12)	4
O(3)	.2289(8)	−.2879(19)	.2614(7)	.76(12)	4
O(4) = $\frac{1}{2}OH^- + \frac{1}{2}O^{2-}$	.4207(9)	.2348(20)	.3058(8)	1.26(14)	4
O(5) = $\frac{1}{2}OH^- + \frac{1}{2}O^{2-}$	.1736(8)	.2626(20)	.4391(8)	.90(12)	4
O(6)	.1290(8)	.2390(19)	.1450(8)	.79(12)	4
O(7)	.5254(9)	.7708(20)	.4379(9)	1.19(14)	4

[a] Estimated errors in parentheses refer to the last decimal place.

[b] Occupancy in unit cell.

coordinates, no sensible relationship existed between initial and final temperature factors. A similar result was encountered for another close-packed structure presently under investigation which was also refined using incomplete and complete sets of data. It is reasonable to state that refinements of close-packed structures may require as complete a set of three-dimensional data as possible, since there are likely to be strong parameter interactions as a consequence of the geometrical restrictions inherent in such structures. Since the isotropic temperature factors can behave much like site population factors during refinement of atomic parameters and since the site population factors can be affected by correlations among atomic parameters, temperature factors obtained for close-packed structures with limited data are probably of little

TABLE 5. INTERATOMIC DISTANCES IN LEUCOPHOENICITE

Estimated standard errors: Me–O ±0.009 Å, O–O′ ±0.013 Å, Me–Me ±0.007 Å

Mn(1)		Mn(2)		Mn(3)		Mn(4)		Si(1)				
2 Mn(1)–O(1)′	2.174 Å	Mn(2)–O(2)	2.167	Mn(3)–O(3)	2.072	Mn(4)–O(5)	2.146	Si(1)–O(7)	1.519	Si–O terminal		
2 –O(6)	2.208	–O(1)	2.188	–O(4)	2.120	–O(4)′	2.186	–O(7)′	1.764	Si–O basal		
2 –O(2)′	2.227	–O(4)	2.223	–O(5)′	2.125	–O(1)′	2.194	–O(5)″	1.771	$\frac{1}{2}$Si–($\frac{1}{2}O^{2-}+\frac{1}{2}OH^{-}$) basal		
average	2.203 Å	–O(6)	2.301	–O(5)′	2.145	–O(7)″	2.214	–O(4)	1.794	$\frac{1}{2}$Si–($\frac{1}{2}O^{2-}+\frac{1}{2}OH^{-}$) basal		
		–O(2)′	2.319	–O(7)′	2.389	–O(3)	2.222	average	1.712			
2O(1)′–O(2)′	2.579[a]	–O(3)	2.351	–O(7)	2.453	–O(6)	2.272					
2O(2)′–O(6)	2.939[b]	average	2.258	average	2.217	average	2.206	O(7)′–O(7)	2.747	O(4)–O(5)″	2.793[a′]	
2O(1)′–O(6)	2.947[b]							O(7)–O(5)″	2.764	O(4)–O(7)′	2.819[a′]	
2O(6)–O(2)″	3.322	O(2)′–O(3)	2.582[a]	O(4)–O(7)′	2.819[a′]	O(1)′–O(3)	2.599[a]	O(4)–O(7)	2.779	O(7)′–O(5)″	2.836[a′]	
2O(6)–O(1)″	3.244	O(2)′–O(6)	2.939[b]	O(5)′–O(7)	2.836[a′]	O(4)′–O(5)	2.793[a′]					
2O(1)′–O(2)″	3.567	O(3)–O(6)	2.948[b]	O(7)′–O(5)′	3.033[b]	O(1)′–O(6)	2.947[b]			average	2.790	
average	3.100	O(4)–O(1)	3.033	O(5)–O(5)′	3.061	O(6)–O(3)	2.948[b]	Si(2)				
		O(2)–O(1)	3.055	O(4)–O(3)	3.063	O(5)–O(7)″	3.033[b]	Si(2)–O(6)	1.612	Si–O terminal		
Si–Mn nearest neighbors		O(2)–O(2)′	3.173	O(4)–O(7)	3.066[b]	O(7)″–O(4)′	3.066[b]	–O(2)′	1.626	Si–O basal		
Si(2)–Mn(1)″	2.784	O(3)–O(4)	3.231	O(7)′–O(7)	3.080[b]	O(6)–O(4)′	3.227	–O(3)	1.644	Si–O basal		
Si(2)–Mn(4)	2.791	O(6)–O(4)	3.247	O(5)–O(3)	3.114	O(1)′–O(7)″	3.239	–O(1)′	1.647	Si–O basal		
Si(2)–Mn(2)″	2.945	O(6)–O(2)	3.291	O(5)–O(7)′	3.229	O(6)–O(5)	3.250	average	1.632			
Si(1)–Mn(4)′	2.748	O(3)–O(1)	3.419	O(5)′–O(3)	3.309	O(3)–O(7)″	3.316					
Si(1)–Mn(3)	2.844	O(2)′–O(1)	3.476	O(7)–O(3)	3.364	O(1)′–O(4)′	3.407	O(2)′–O(3)	2.582[a]	O(3)–O(6)	2.727	
Si(1)′–Mn(3)	2.864	O(2)–O(4)	3.654	O(5)–O(4)	3.379	O(3)–O(5)	3.471	O(1)′–O(2)′	2.579[a]	O(2)′–O(6)	2.731	
		average	3.171	average	3.113	average	3.108	O(1)′–O(3)	2.599[a]	O(1)′–O(6)	2.738	
										average	2.659	

[a] Si(2)–Mn shared edges [a′] Si(1)–Mn shared edges [b] Mn–Mn shared edges

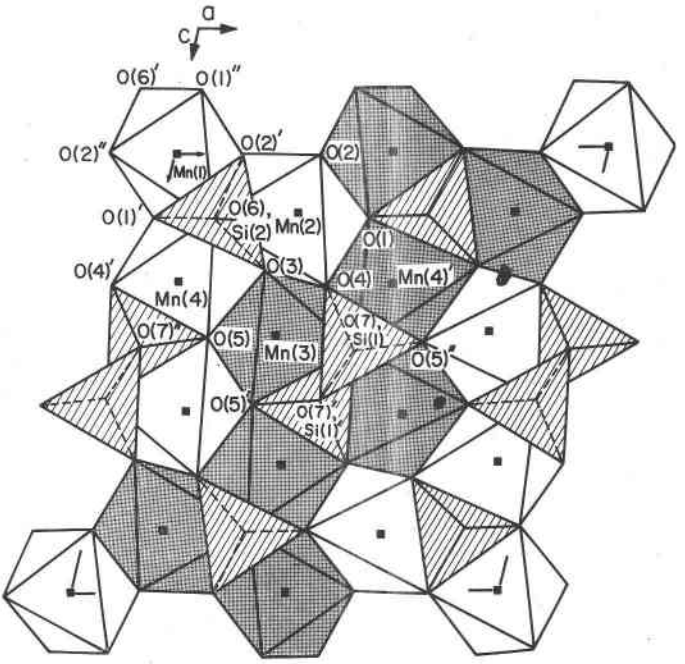

FIG. 1. Polyhedral diagram of the leucophoenicite crystal structure, projected down the y-axis. The atomic species are labelled in conformity with the text: unprimed labels are the atomic positions in Table 4 and primed labels are their symmetry equivalents. Silicon atoms reside in the centers of the ruled tetrahedra. Unshaded octahedra are at $y \sim 0$, stippled octahedra at $y \sim 1/2$.

physical meaning. Informative in this aspect would be a more detailed study of parameter interactions in close-packed structures in general.

Final atomic coordinates and isotropic temperature factors are given in Table 4. Interatomic distances are presented in Table 5 and the observed and calculated structure factor amplitudes appear in Table 6.[1]

DISCUSSION OF THE STRUCTURE

Octahedral and Tetrahedral Topology. One unit cell of the leucophoenicite atomic arrangement is depicted as a polyhedral diagram in Figure 1. It consists of hexagonal close-packed oxygen atoms with the octahedral populations equally divided between the two octahedral cation levels

[1] To obtain a copy of Table 6, order NAPS Document No. 01051 from ASIS National Auxiliary Publications Service, c/o CCM Information Corporation 909 Third Avenue, New York, New York, 10022; remitting $2.00 for microfiche or $5.00 for photocopies, payable to CCMIC-NAPS.

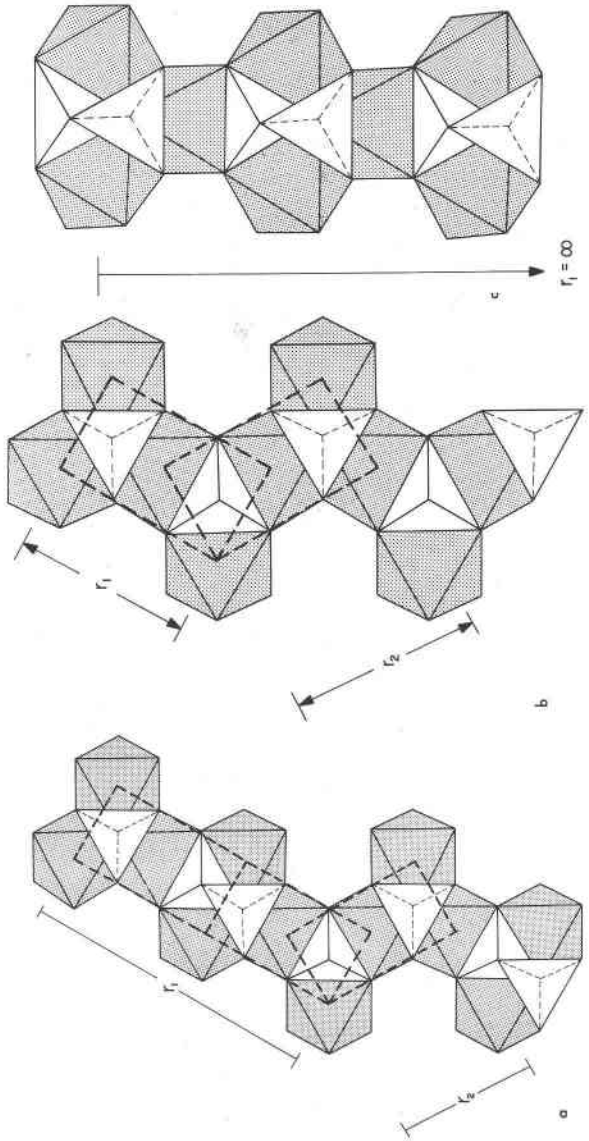

FIG. 2. a. The leucophoenicite chain with the overlying tetrahedra. The octahedral 5-clusters are dashed, with r_1 and r_2 defining the two segments comprising the chain motif. b. The olivine chain. Note that no tetrahedra occur pairwise. c. The hypothetical chain for $\cdots r_1 r_2 \cdots = \cdots \infty \mathrm{O} \cdots$. Note that all tetrahedra occur pairwise.

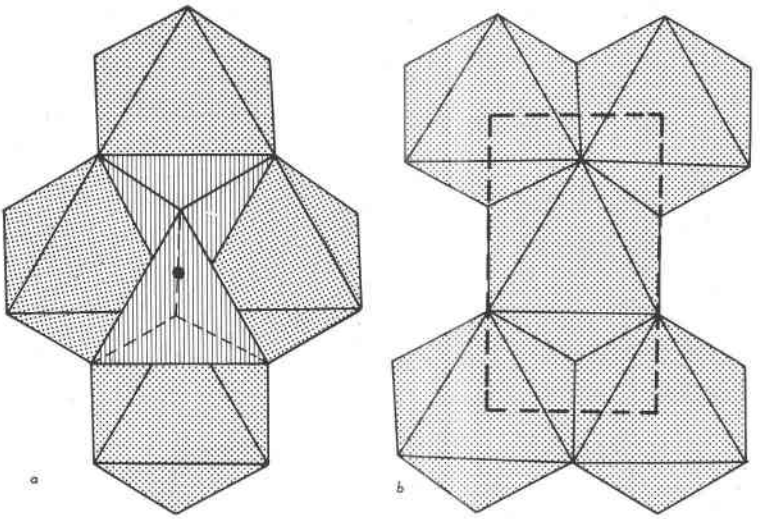

FIG. 3. a. Octahedral 4-cluster with overlying tetrahedral pair. The solid circle represents the inversion center situated at the midpoint of the tetrahedrally shared edge. b. Octahedral 5-cluster, the component of the algorithm defining the serrated chains.

along the *b*-axis repeat. The octahedra share edges and corners and, when projected down the *b*-axis, are equivalent to the tessellation of hexagons with equally weighted populations of oxygen atoms at the nodes and of manganese atoms in the centers of the hexagons, since Mn:O=1:2. This is a general property for all hexagonal close-packed structures, the only necessary conditions being half of the octahedral sites populated and the absence of face-sharing between octahedra. A tetrahedral population occurs whenever a trigonal triplet of octahedra in one of the two levels has three triangular edges available for sharing with the tetrahedral base. These features are also underlying principles in the related structures of the olivine and humite groups.

The octahedral populations are kinked serrated chains of alternate one- and two-octahedra which run parallel to the *z*-axis (Figure 2a). Since the composition of leucophoenicite is isotypic to humite, this arrangement constitutes a new structure type and differs from the kinked serrated chains found in the olivine and humite structures. Thus, leucophoenicite does not belong to the same structural algorithm as does the humite group and we shall see that the general humite formula, $nM_2SiO_4 \cdot M(OH)_2$, where M are octahedral cations, does not strictly apply to this mineral.

One remarkable and peculiar feature arises from the leucophoenicite octahedral arrangement. From a polyhedrist's viewpoint, whenever a cluster of four octahedra appears, as depicted in Figure 3a, a tetrahedron

can be either placed with its base *above* the octahedral triplet or with its base *below* the alternative triplet centrosymmetrically situated from the former. Since both triplets are equivalent, this means that one triplet site is as likely to be populated as the other from an energetic standpoint. For hexagonal close-packed octahedral two-layer repeat structures, this would result in occupied tetrahedral edge-sharing whenever a center of symmetry occurs as defined in Figure 3a. For reasonably ionic compounds like the nesosilicates, such an arrangement, if possessing fully occupied sites, would be highly unstable. Indeed, it is arrangements like this that crystallographers tend to exclude in the early stages of structure analysis using packing models. In the leucophoenicite structure, these sites are exactly half-occupied on the average, fulfilling the humite-like stoichiometry while avoiding local edge-sharing between occupied tetrahedra. For an electrostatically balanced system, the replacement $Si \rightarrow \square$ implies $O^{2-} \rightarrow OH^-$, where $\square$ is a hole. In this manner, O^{2-} is coordinated by $3Mn^{2+} + Si^{4+}$ and OH^- by $3Mn^{2+}$, resulting in a locally neutral system, exactly analogous to the olivine and humite minerals. This disordered tetrahedral pair has average composition $[(SiO_4)\ (OH)_2]^{6-}$; the point symmetry at the midpoint of the shared edge is $\bar{1}$.

The remaining independent Si tetrahedral site is fully occupied and has point symmetry 1. The octahedral clusters around this site are trigonal triplets, locally arranged in a manner analogous to olivine. The crystallochemical formula for leucophoenicite is interpreted as

$$Mn_7[SiO_4]_2[(SiO_4)(OH)_2].$$

Though disorder of O^{2-} and OH^- groups over equivalent sites is hardly new to science, the arrangement found in leucophoenicite is rather noteworthy. To my knowledge, it is unique in having partly occupied edge-sharing tetrahedra for a silicate structure. Consequently, humite-like stoichiometries are possible for arrangements *not* belonging to the humite homologous series. An infinite series of novel kinked serrated chains can be conceived since the clusters in Figure 3a which make up the chains found in leocophoenicite are capable of an infinite variety of zig-zag connections.

To evolve a family of kinked serrated chains, consider the cluster of five octahedra illustrated in Figure 3b. This cluster is not only the basis of the leucophoenicite chain in Figure 2a but also is the basis of the olivine structure type. Each of the dashed boxes in Figure 2a outlines a cluster. It is seen that a collection of two successive five-clusters in one direction followed by one five-cluster in the other direction yields the principal motif of the leucophoenicite octahedral chain. This may be

symbolized as $\cdots r_1 r_2 \cdots$, where r_1 denotes the number of clusters in one direction followed by r_2 clusters in the other direction. Thus, leucophoenicite is $\cdots$ 21 $\cdots$. The arrangement $\cdots$ 11 $\cdots$ is olivine (Figure 2b) and is the simplest of the kinked serrated chains. Since no octahedral four-clusters of the type in Figure 3a can be found, olivine does not exhibit edge-sharing partly occupied tetrahedra. The arrangement $\cdots \infty O \cdots$, a serrated chain with no kinks, is particularly interesting (Figure 2c), since all tetrahedra occur pairwise. Its stoichiometry for a hypothetical manganese silicate is Mn_3 $[(SiO_4)$ $(OH)_2]$ and is dimorphous to the norbergite structure type. Its cell has $a \sim 9.0$, $b \sim 4.8$, $c \sim 5.3$ Å, space group $Pmnn$, $Z=2$. Actually, the octahedral arrangement in this hypothetical structure is identical to that of kotoite, $Mg_3B_2O_6$. No tetrahedral shared edges occur in this compound since the anionic units are $(BO_3)^{3-}$ triangles. The kotoite structure is reported in Ito (1950).

These sequences may be quite complicated before the chain motif repeats itself and in general we have $\cdots r_1 r_2 r_3 \cdots r_n \cdots$. Evidently, even indices define one direction and odd indices the other. The number of paired tetrahedra within a sequence is $(r_1-1)+(r_2-1)+(r_3-1)+\cdots+(r_n-1)=\sum_n r_n - n$. Thus, for any motif, the amount of OH^- and the general stoichiometry can be obtained since one tetrahedral pair is crystallochemically $[(SiO_4)$ $(OH)_2]$. The general stoichiometry, then, is

$$X_{3\sum_n r_n - n}[SiO_4]_{\sum_n r_n}[OH]_{2(\sum_n r_n - n)}$$

where X are the divalent octahedral cations. This general formula describes the leucophoenicite homologous series, distinct from the humite homologous series, which is $pX_2SiO_4 \cdot X(OH)_2$. Both series have olivine in common, since this structure type is the simplest and the only anhydrous arrangement in both series.

Relation to Crystal Morphology and Twinning. Palache (1928) chose the morphological cell a:b:c = 1.1045:1:2.3155, $\beta = 103°16'$ based on his goniometric measurements of fifteen crystals. This is to be compared with $a:b:c = 2.2466:1:2.3465$, $\beta = 103°56'$, derived from the structure cell in this study (Table 2). Evidently, the transformation from the morphological cell to the X-ray cell requires a doubling of Palache's a-value.

A third cell was chosen by Moore (1967) for Palache's crystals, which is pseudo-orthogonal; it requires the transformation $a'=a$, $b'=b$, $c'=4c+a$, based on the X-ray cell. This cell was chosen since it was then believed that leucophoenicite might be structurally closely related to humite. In that paper, I stated that the cell is B-centered; this is not entirely correct since the cell has in addition two extra lattice nodes,

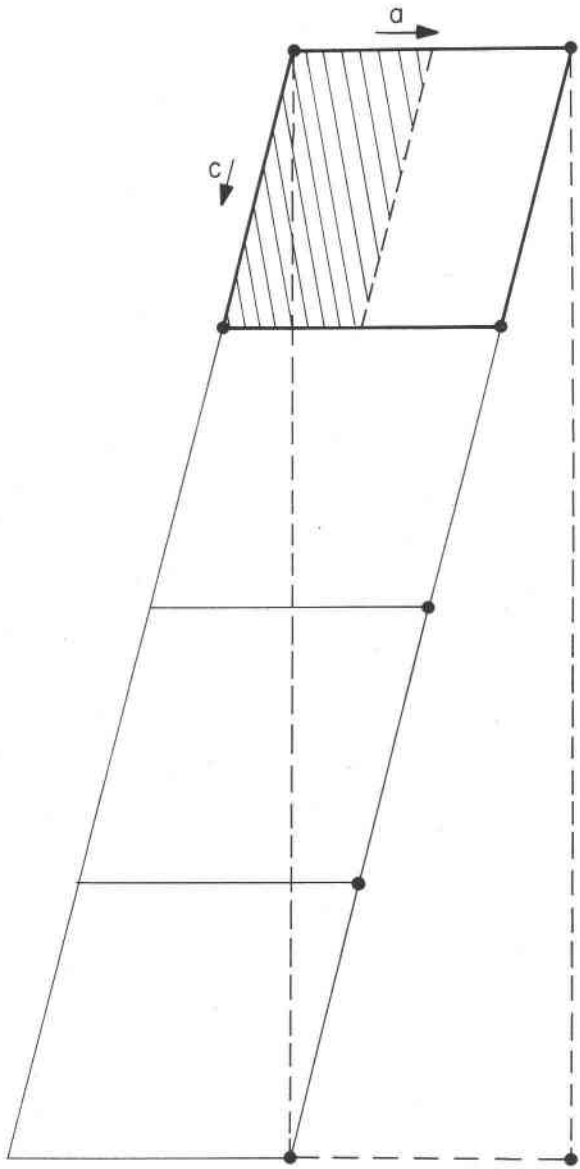

FIG. 4. Three unit cells used in studies on leucophoenicite. The ruled cell is the morphological cell of Palache (1928). The outlined cell with nodes at the vertices is the structure cell in this paper and the dashed cell is the pseudo-orthogonal "B"-cell of Moore (1967).

TABLE 7. MORPHOLOGICAL ANALYSIS OF LEUCOPHOENICITE

Symbol (X-ray cell)	Violations[a]	Form	Frequency[b]
001		(*c*)	11
100	x		
$\bar{1}01$	x		
101	x		
002	x		
$\bar{1}02$	x		
$\bar{2}01$		(*r*)	12
200		(*a*)	10
010	x		
102	x		
011		(*o*)	9
$\bar{2}02$		(*i*)	10
110		(*s*)	6
201		(*e*)	8
$\bar{1}11$		(*u*)	6
111		(*j*)	1
$\bar{1}03$	x		
003	x		
$\bar{3}01$	x		
012		(*f*)	2
$\bar{1}12$		(*q*)	2
$\bar{2}11$		(*p*)	2
210		(*m*)	2
300	x		
$\bar{2}03$		(*y*)	7
202		(*l*)	4

[a] $h01$ $h \neq 2n$, $0k0$ $k \neq 2n$. Higher order symbols, already accounted for, are included as violations. The violations are designated "x".

[b] Based on fifteen crystals. The form letters are Palache's (1928), retained in Moore (1967). Not included are (*b*)11, (*k*)4, (*x*)5, (*d*)6, (*l*)7, (*z*)4, (*h*)2, (*n*)6.

bringing the multiplicity to 4. The relative orientation of the three cells is shown in Figure 4. Fortunately, the extinction criteria used in the morphological analysis satisfy this complex cell, leaving the analysis correct, though cumbersome. Cook (1969) points out that Palache's fifteen crystals were not solely leucophoenicite, but included sonolite as well. The relationship in cell criteria between the two minerals is similar —sonolite has *a* 10.7, *b* 4.85, *c* 14.3 Å, $\beta = 100.5°$, $P2_1/a$. Hence, composite morphological data of the two species would be difficult to distinguish. In any event, a revision of form frequency is given in Table 7, based on the leucophoenicite X-ray cell of this paper. The relative frequencies are essentially the same as those given in my previous paper;

although the data are presumably composites of leucophoenicite and sonolite, the similarity in cell criteria between the two minerals would lead to similar conclusions in either case.

Leucophoenicite is frequently twinned, the twin plane invariably being {001}. This is explained on the basis of the crystal structure. Writing a segment of the chain as its component $\cdots$ 12121212 $\cdots$ implies that the sequence $\cdots$ 12122121 $\cdots$ differs only in the addition of a twin boundary. Since the chains run parallel to the z-axis, this twin boundary must be the {001} plane. Polysynthetic twinning, on {001}, of the order of cell dimensions, leads to the pseudo-orthogonal cell mentioned above with orthorhombic intensity distribution. This cell is B-centered and possesses the extinction criteria mentioned in Moore (1967, p. 1231). By assuming this pseudo-orthogonal cell, the space group *Bmam* can be obtained, though additional systematic absences are present as a consequence of the twinning geometry. Thus Moore's "*o*-leucophoenicite" can be readily explained on the basis of polysynthetic twinning on {001}. Massive pink leucophoenicite from Franklin, New Jersey and brown leucophoenicite ("hydrotephroite") from Pajsberg, Sweden yield the twinned cell in single crystal examination. Another 'polytype' proved to be sonolite twinned on {001}. The twinning relationships and cell orientations of the humite group minerals have been recently discussed by Jones (1969) whose results parallel those observed for leucophoenicite. The positive quadrants of the reciprocal lattice of twinned leucophoenicite and sonolite are depicted in Figure 5. Since all hexagonal close-packed two-layer repeat structures which have one crystallographic axis normal to the close-packed layers can be ultimately transformed into pseudo-orthogonal cells, the problems encountered in humite and leucophoenicite twinning are largely aspects of the general problem of epitaxial overgrowth and twinning in close-packed systems.

Nomenclature. The only previous suggestion of a leucophoenicite nomenclature was by Moore (1967) where I casually designated the monoclinic members as "*m*-leucophoenicite" and the orthorhombic as members "*o*-leucophoenicite." The foregoing discussion clearly indicates that such a nomenclature is not necessary, since all carefully investigated leucophoenicites are actually the monoclinic member. The manganese isotype of humite does not belong to the leucophoenicite group and accordingly it has been treated as a new and distinct species. There remain additional incompletely investigated variants: Moore (1967) mentions examples of variants which yield complex streaked photographs and distinct powder patterns, and Cook (1969) reports related compounds with distinct powder photographs. More detailed study will be necessary to establish

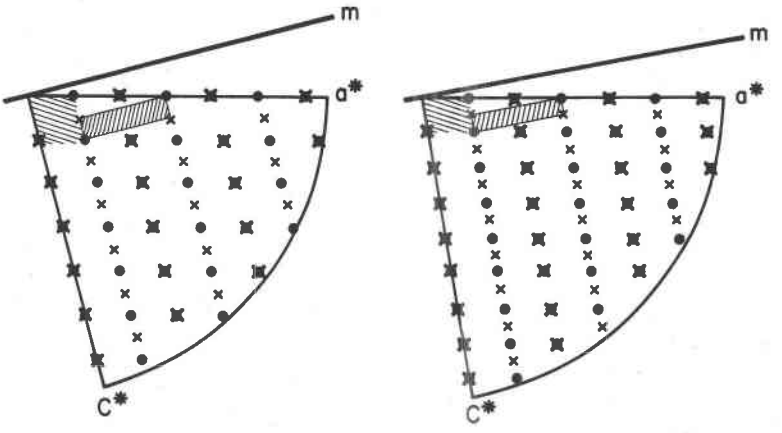

FIG. 5. Reciprocal net a^* c^* down the b-axis for leucophoenicite and sonolite, twinned by reflection on {001}. The twin plane is drawn bold. Reflections of the $h0l$ level are drawn as circles; for hkl, they are drawn as crosses.

their relationship with leucophoenicite and the humites. Perhaps some of these compounds will prove to be members of the homologous series discussed herein.

Leucophoenicite structures are defined as any members which fulfill the following criteria: (1) chains made up of the octahedral five-cluster which allows them to be designated according to the algorithm presented previously, (2) identical chains in the two octahedral levels within the 4.8 Å repeat, and (3) chains other than $\cdots 11 \cdots$ (olivine) which require the presence of some hydroxyl groups and disordered edge-sharing tetrahedra. If such compounds are discovered, their designation can be conveniently referred to the algorithm. It must be emphasized that this series is not a polytypic one in the strict sense of the term, since each hypothetical member has a specific quantizable composition distinct from the others.

INTERATOMIC DISTANCES

There are four manganese, two silicon, and seven oxygen atoms in the leucophoenicite asymmetric unit. One manganese atom is fixed at the cell origin. Thus, there are twenty-one independent Mn–O distances and eight independent Si-O distances (Table 5). The Mn–O distances average Mn(1)–O 2.20, Mn(2)–O 2.26, Mn(3)–O 2.22, and Mn(4)–O 2.21 Å

which, excepting Mn(2)–O, are within the range of Mn^{2+}–O average octahedral distances generally observed in mineral structures. Since the Mn(2)–O octahedron is the largest of the four, it probably accommodates Ca^{2+} reported in the chemical analyses. Similarity in the scattering powers of Mn and Ca does not permit a definite site preference scheme for minor Ca on the basis of crystal structure analysis; the refined isotropic temperature factors for the Mn atoms in Table 4 do not differ significantly.

Like the olivine and humite structures, the Si–O tetrahedra share three nearly triangular edges with free edges of the octahedral trigonal triplets. Similar to these structures, the Si–O apical distance (the distance opposite the shared edges) is significantly shorter, as a consequence of Mn(Mg)–Si cation-cation repulsions. The Mn(1) octahedron shares two edges with Si-O tetrahedra and four with octahedra, the Mn(2) octahedron shares one with a tetrahedron and two with octahedra, the Mn(3) octahedron shares two with tetrahedra and two with octahedra and the Mn(4) octahedron shares two with tetrahedra and four with octahedra. Listing the O–O′ polyhedral distances in the order of increasing interatomic distances shows the effect of the cation-cation repulsions on the relative foreshortening of the shared edges (Table 5): the O–O′ distances associated with edge-sharing octahedra range from 2.94 to 3.08 Å, whereas the average O–O′ polyhedral distances range from 3.10 to 3.18 Å.

The half-populated tetrahedral edge-sharing doublets (Si(1)–O) offer some unusual features. It must be emphasized that the three-dimensional refinement led to good convergence in atomic positions and isotropic temperature factor for a tetrahedral site half-populated with silicon, and that an ensuing three-dimensional difference synthesis failed to reveal any positive or negative regions substantially above background level around this site. This means that the Si average position is fairly well-localized within the structure and that the Si(1)–O distances are of some physical meaning. O(4) and O(5), two of the basal distances associated with the Si(1)–O tetrahedron, are on the average $\frac{1}{2}O^{2-}+\frac{1}{2}OH^{-}$, depending on whether Si(1) is present or absent at its site. Suggestive of this averaging are the relatively high temperature factors for O(4), 1.3 $Å^2$ and O(5), 0.9 $Å^2$. Typical isotropic temperature factors for O^{2-} in close-packed systems are in the range 0.4 to 0.7 $Å^2$.

To illustrate the effect of the Si(1) half occupancy on O(4) and O(5), a difference synthesis ρo-ρc was performed with these three atoms omitted in the calculation. Sections through O(4) and O(5) are shown in Fig. 6. It is seen that these sections are elliptical in outline, with the major axes running parallel to the line connecting Si(1)–Mn(2) for O(4) and Si(1)–Mn(3) for O(5). The elliptical shape of electron density

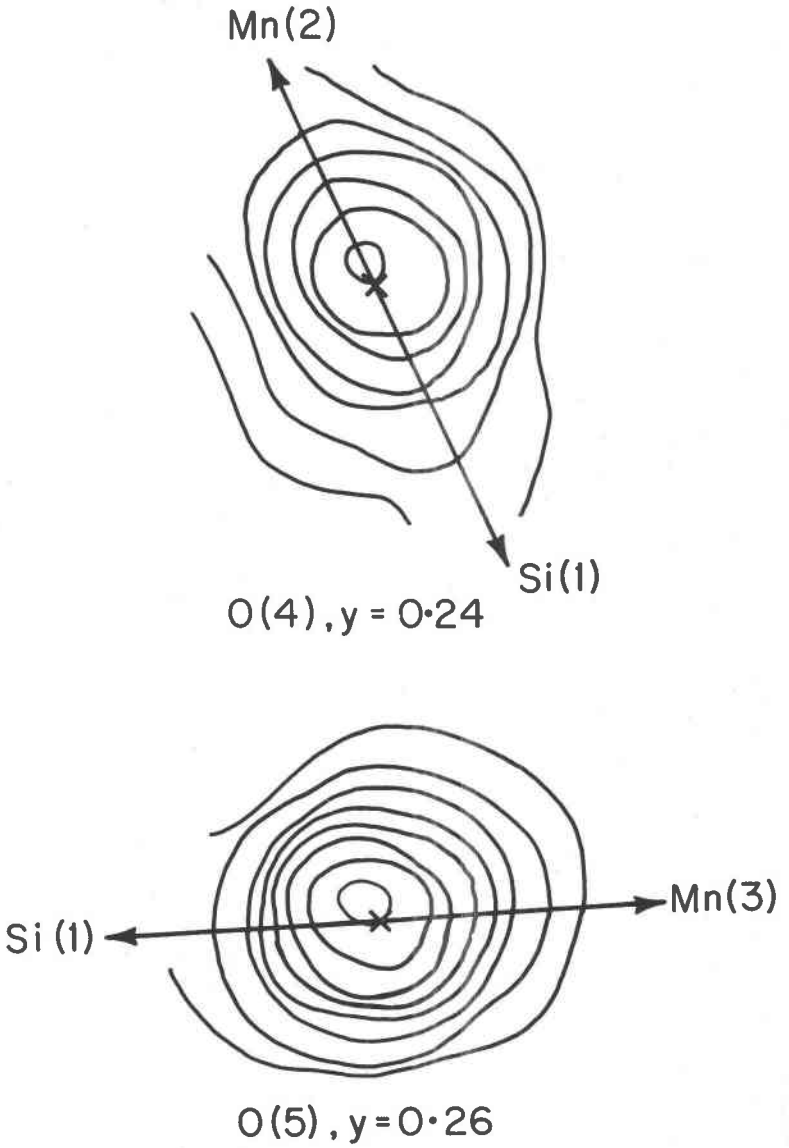

FIG. 6. Difference synthesis sections through O (4) and O(5). These atoms were omitted in the calculation. The atom centers obtained from least-squares refinement are shown by 'X'. The lines between Si(1) and neighboring Mn(2) and Mn(3) are shown.

sections is interpreted as an average of two O(4) and two O(5) positions only slightly displaced from their mean central positions as a result of the Si(1) half occupancy.

O(7) and its inversion, O(7)′, define the tetrahedral shared edge and O(7) is therefore O^{2-} since an average of one Si atom as well as three Mn atoms coordinate to it. The apical distance Si(1)–O(7) 1.52 Å is unusually short, with the three long basal distances each with 1.77 Å. The

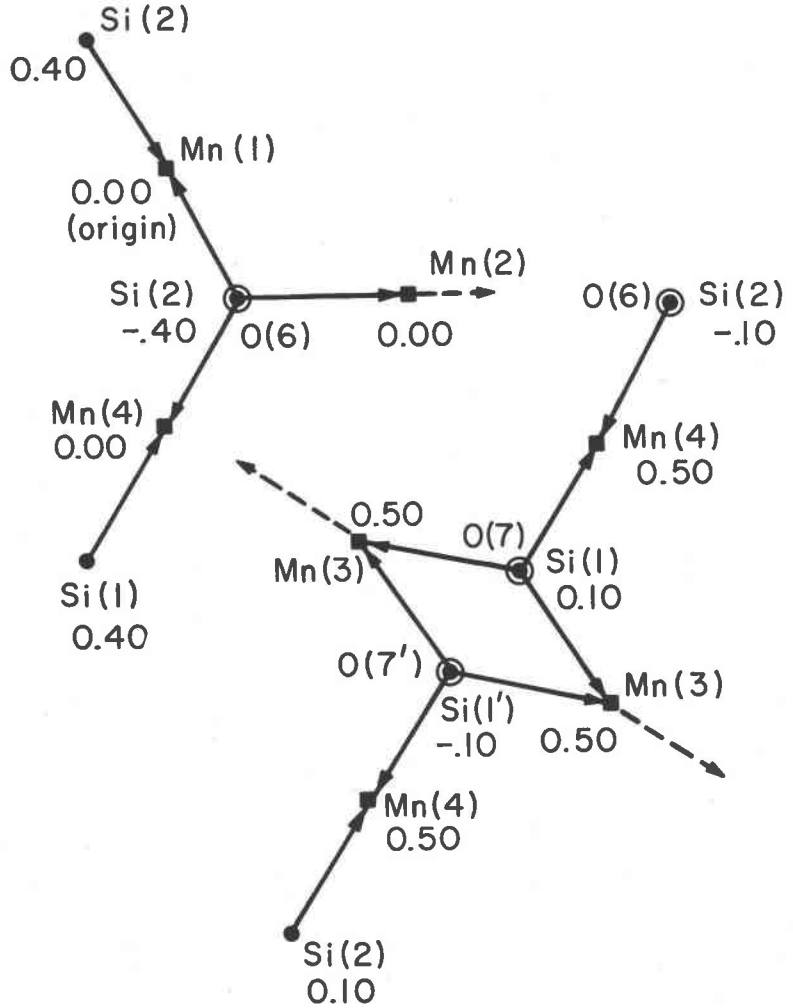

FIG. 7. Si→Mn repulsion diagram for leucophoenicite. Directions of net repulsion are dashed.

average Si(1)–O 1.71 Å distance is substantially larger than Si(2)–O 1.63 Å in leucophoenicite, 1.63 Å in norbergite (Gibbs and Ribbe, 1969) and 1.64 Å for a fayalite (Birle, Gibbs, Moore and Smith, 1968).

The O(7)–O(7)′ Shared Edge. The apical and basal Si(1)–O(7),–O(7)′ distances are 1.52 and 1.77 Å respectively. These two distances are perhaps the most unusual features of the crystal structure, although they are readily explained as the effects of cation-cation repulsions. If cation-cation repulsions are represented as vectors originating from the silicon atoms and terminating at the neighboring manganese atoms, it is seen that the net repulsions of the manganese atoms are away from the apical oxygens (Figure 7). Consequently, the Mn–O apical distances are longer than average (Table 5), leaving the apical oxygen relatively undersaturated with respect to cations. Thus, the Si–O apical distances are relatively short. For the O(7) apical oxygen associated with Si(1), this effect is particularly violent since Mn(3) is additively repelled away from the apical O(7) position by Si(1) and its inversion Si(1)′. The argument is made complete with the observation that the resulting Mn(3)–O(7) 2.39 and Mn(3)–O(7)′ 2.45 Å distances are unusually long. These repulsions also induce the long Si(1)–O(7)′ 1.76 Å basal distance; consequently O(7) is severely undersaturated on the average, and local electroneutrality is assured by the short Si(1)–O(7) distance.

Based on this unusual tetrahedral arrangement, it is remarkable that leucophoenicite exists as a fairly stable phase. The peculiar arrangement of edge-sharing tetrahedra in this species may result from the close-packed nature of the structure and, consequently, the possible control of the octahedral populations over tetrahedral populations. Disordered atoms in close-packed arrangements are frequently encountered in natural and synthetic systems. Though progress is being made in the systematic topologic analysis of close-packed arrangements, no present theory is available to derive *a priori* the stable octahedral and tetrahedral populations; such a theory would have profound influence in our general knowledge of cation distributions in reasonably ionic dense-packed arrangements.

ACKNOWLEDGEMENTS

The following persons offered valuable assistance in this study: Mrs. Eva Browder who helped in the data collection, Dr. S. J. Louisnathan who assisted in the cell edge refinements, Mr. J. K. Nelson who supplied leucophoenicite crystals from his private collection, and Dr. E. Olsen of the Field Natural History Museum who offered the crystal used in this study. Especial thanks is extended Prof. P. H. Ribbe who read the revised manuscript prior to its submission and Mr. G. R. Zechman who provided detailed electron probe microanalyses on the crystal used in the X-ray study.

This study was made possible by the NSF grant GA-907 and an Advanced Research Projects Agency grant awarded the University of Chicago.

References

Birle, J. D., G. V. Gibbs, P. B. Moore, and J. V. Smith (1968) Crystal structures of natural olivines. *Amer. Mineral.* **53,** 807–824.

Cook, D. (1969) Leucophoenicite, alleghenyite and sonolite from Franklin and Sterling Hill, New Jersey. *Amer. Mineral.* **54,** 1392–1398.

Gibbs, G. V., and P. H. Ribbe (1969) The crystal structures of the humite minerals: I. Norbergite. *Amer. Mineral.* **54,** 376–390.

Ito, T. (1950) *X-ray Studies on Polymorphism.* Maruzen Co. Ltd., Tokyo, 143–150.

Jones, N. W. (1969) Crystallographic nomenclature and twinning in the humite minerals. *Amer. Mineral.* **54,** 309–313.

MacGillavry, C. H. and G. D. Rieck, eds. (1962) *International Tables for X-ray Crystallography, vol. 3.* Kynoch Press, Birmingham, 202–204.

Moore, P. B. (1967) On leucophoenicites: I. A note on form developments. *Amer. Mineral.* **52,** 1226–1232.

——— (1968) The crystal structure of chlorophoenicite. *Amer. Mineral.* **53,** 1110–1119.

Palache, C. (1910) Beitrag zur Mineralogie von Franklin Furnace, New Jersey. *Z. Krystallogr. Mineral.* **47,** 584–585.

——— (1928) Mineralogical notes on Franklin and Sterling Hill, New Jersey. *Amer. Mineral.* **13,** 297–329, especially 315.

——— (1935) The Minerals of Franklin and Sterling Hill, Sussex County, New Jersey, *U.S. Geol. Surv. Prof. Pap.* **180,** 104–105.

Penfield, S. L. and C. H. Warren (1899) Some new minerals from the zinc mines at Franklin, New Jersey. *Amer. J. Sci., 4th series,* **8,** 351–353.

Manuscript received, May 9, 1968; accepted for publication, March 12, 1970.